Applied Surface Science 311 (2014) 574–581

Contents lists available at ScienceDirect

Applied Surface Science

journal homepage: www.elsevier.com/locate/apsusc

Fabrication, characterization, and photocatalytic performance of exfoliated g-C_3N_4–TiO_2 hybrids

Fei Chang[a,*], Jian Zhang[a], Yunchao Xie[a], Juan Chen[a], Chenlu Li[a], Jie Wang[a], Jieru Luo[a], Baoqing Deng[a], Xuefeng Hu[b,*]

[a] School of Environment and Architecture, University of Shanghai for Science and Technology, Shanghai 200093, PR China
[b] Key Laboratory of Coastal Zone Environmental Processes and Ecological Remediation, Yantai Institute of Coastal Zone Research, Chinese Academy of Sciences, Yantai 264003, Shandong, PR China

ARTICLE INFO

Article history:
Received 18 March 2014
Received in revised form 18 May 2014
Accepted 18 May 2014
Available online 26 May 2014

Keywords:
Exfoliated g-C_3N_4 nanosheets
TiO_2
Hybrid
Photocatalyst
Mechanism

ABSTRACT

A series of TiO_2 hybrids composited with exfoliated g-C_3N_4 nanosheets (CNs) were successfully synthesized through a facile sol–gel method and fully characterized by X-ray diffraction patterns (XRD), Fourier transform-infrared spectroscopy (FT-IR), X-ray photoelectron spectroscopy (XPS), transmission electron microscopy (TEM), scanning electron microscopy (SEM), and UV–vis diffuse reflectance spectra (UV–vis DRS). The CNs–TiO_2 hybrids were exposed to visible light irradiation and showed much higher catalytic capability toward degrading dye rhodamine B (RhB) comparing with bare TiO_2 and N-TiO_2. The sample CNs–TiO_2-0.05 exhibited the largest apparent reaction rate constant among all CNs–TiO_2 hybrids, which was 2.4 times and 7.0 times as high as bare TiO_2 and N-TiO_2, respectively. The enhanced catalytic efficiency could be mainly attributed to the well-matched band gap structure with heterojunction interface, suitable specific surface area, and favorable optical property. In addition, active species trapping experiments were conducted, revealing that photoinduced holes (h^+) had a severe influence on catalytic outcome, through which a possible catalytic mechanism was finally realized and proposed.

1. Introduction

Semiconductor photocatalysis is one promising and extensively researched technique in the field of environmental remediation and renewable energy supply [1]. Among all semiconductors used as photocatalysts, TiO_2 has attracted much attention from numerous researchers due to those favorable physicochemical properties [2]. However, TiO_2 fails to catalyze degradation of environmental contaminations upon visible light irradiation and can only exert photocatalysis in presence of ultraviolet light that takes up merely 4% of solar energy, attributing to the large band gap energy of 3.2 eV [2,3]. In addition, high recombination rate of photoinduced hole–electron pairs is another factor limiting its practical applications. As a result, abundant efforts have been devoted to advance TiO_2 through structural modifications with metallic [4,5], nonmetallic elements [6,7], and other semiconductors [8,9], aiming to produce photocatalysts with both merits of visible light response and efficient separation of hole–electron pairs.

Graphitic carbon nitride (g-C_3N_4) is normally prepared through pyrolysis of nitrogen-rich organic precursors and thus no metallic species are remained in structure after synthesis [10]. g-C_3N_4 owns intrinsic characteristic structure units called tri-*s*-triazine and is recognized as the most stable allotrope of carbon nitride [11]. Moreover, it was reported that g-C_3N_4 could promote the hydrogen generation by water splitting under visible light illumination, which inspired researchers to further explore modification of g-C_3N_4 structures with enhanced photocatalytic performance [12]. An efficient strategy is to exfoliate g-C_3N_4 in bulk form to corresponding nanosheets by means of diverse methods [13–16]. During exfoliation, multilayer structure is destroyed to create numerous thin sliced fragments with enlarged specific surface area exposed. Thin sliced structure benefits the efficient transfer and separation of photoinduced charge carries, and enlarged specific surface areas supply abundant actives sites exposed and large visible light adsorption, thus remarkably improving the photocatalytic capability [17].

Several investigations have reported that composites of bulk g-C_3N_4 and TiO_2 could be constructed to pursue visible light response and satisfactory photocatalytic efficiency since band gap

* Corresponding authors at: School of Environment and Architecture, University of Shanghai for Science and Technology, Jun Gong Road 516 No., Shanghai, PR China. Tel.: +86 21 55271722/+86 535 2109157.
E-mail addresses: feichang@usst.edu.cn (F. Chang), xfhu@yic.ac.cn (X. Hu).

http://dx.doi.org/10.1016/j.apsusc.2014.05.111
0169-4332/

structures of both semiconductors are well matched and readily form heterojunction interfaces along boundaries [3,18–22]. Yan et al. reported that g-C_3N_4–TiO_2 composites prepared in a direct grind manner could catalyze hydrogen evolution under visible light [3]. Miranda et al. demonstrated that g-C_3N_4–TiO_2 composites by a simple impregnation method exhibited improved photocatalytic activity upon degradation of phenol [19]. Zhao et al. indicated that g-C_3N_4–TiO_2 hybrid by a hydrolysis approach could efficiently remove phenol in visible light [20]. Yu et al. synthesized Z-scheme g-C_3N_4–TiO_2 photocatalysts for efficient removal of formaldehyde in air [21]. Boonprakob et al. fabricated g-C_3N_4–TiO_2 films that showed enhanced photocatalytic efficiency on dye methylene blue [22]. To date, researchers have only focused on the synthesis and photocatalytic evaluation of TiO_2 hybrids with bulk g-C_3N_4 and no report relevant to TiO_2 hybrids with exfoliated g-C_3N_4 has been found, even virtues of exfoliated g-C_3N_4 are fully realized. As a result, in this study a series of CNs–TiO_2 hybrids were first fabricated and characterized with a collection of analytic techniques. These CNs–TiO_2 hybrids were featured with enlarged specific surface areas, favorable optical feature, and intimate interface between both TiO_2 and CNs semiconductors and thus showed marvelously enhanced photocatalytic capability over dye RhB degradation upon visible light irradiation in comparison with bare TiO_2 and N-TiO_2. In addition, active species trapping experiments were also conducted to understand photocatalytic mechanism and photoinduced holes (h^+) exerted a main effect on catalytic process in this study.

2. Materials and methods

2.1. Materials

All chemicals involved were purchased from Sinopharm Chemical Reagent Co., Ltd. (China) and used directly for experiments without any further purification. Aqueous solutions utilized were prepared with deionized water.

2.2. Synthesis of exfoliated CNs

The CNs was prepared according to the reference with small modification [16]. A typical synthesis was described as follows: a desired amount of melamine was put into a semi-closed alumina crucible and annealed in a muffle furnace at 550 °C for 4 h. After cooling down to an ambient temperature, yellow polymeric g-C_3N_4 in bulk form was obtained. Then bulk g-C_3N_4 loaded on an open alumina crucible was annealed in a muffle furnace at 500 °C for 2 h to supply exfoliated CNs as a light yellow powder.

2.3. Fabrication of CNs–TiO_2 hybrids

The synthetic procedure of CNs–TiO_2 hybrids was depicted as below. A certain amount of CNs was added into isopropanol (40 mL) and the resultant suspension was vigorously stirred at ambient temperature for 2 h prior to addition of tetra-*n*-butyl titanate (4 mL). After stirring for 3 h, deionized water (40 mL) was added into the above mixture in dropwise and the obtained milky liquid stood in a drying oven for 24 h at 60 °C to give a powder, which was collected and annealed at 400 °C for 1 h to give target CNs–TiO_2 hybrids, denoted as CNs–TiO_2-*X*, where *X* referred to the mass percentage of CNs in CNs–TiO_2 hybrids. Bare TiO_2 synthesized using a same protocol in the absence of CNs and N-doped TiO_2 (N-TiO_2) prepared using a previously reported procedure [23] were adopted as references.

2.4. Characterization

The crystal structures of samples were investigated using a Bruker D8 Advance X-ray diffractometer with Cu *K*α radiation. Optical property was recorded on a Shimadzu UV2600 UV–vis spectrophotometer with $BaSO_4$ as a reflectance standard. Nitrogen adsorption–desorption isotherms at 77 K of samples were measured by a Tristar Π3020 nitrogen adsorption apparatus. All samples were degassed at 473 K for 2 h before measurement. X-ray photoelectron spectroscopy (XPS) was performed on a Thermo ESCALAB 250Xi system to analyze oxidation states and surface chemical composition of samples. The C 1s signal was set to 284.8 eV for calibration. The micro morphologies were observed by transmission electron microscopy (TEM) conducting on a FEI Tecnai G2 20 electron microscope with an acceleration voltage of 200 kV and scanning electron micrographs (SEM, Hitachi Electronic S4800). The FT-IR spectra were conducted on a Bruker V-70 Fourier transform-infrared spectrophotometer using KBr pellet as the reference.

2.5. Photocatalytic activity test

The visible light irradiation was obtained by a 400 W halide lamp (Institute for Electric Light Sources, Beijing) with a 2 M sodium nitrite solution as a filter to cut off ultraviolet light (<400 nm) and to eliminate thermal effect [24]. Forty milligram of photocatalysts and 40 mL of RhB (10 mg/L) solution were added into a quartz glass tube set in a LIMX-VII apparatus manufactured by Bylabo Precision Instrument Co. Ltd. (Xi'an, China). Before exposure to visible light irradiation, the suspension was magnetically stirred in dark for 1 h to attain the desorption–adsorption equilibrium. During reaction, a magnetic stirrer was employed for continuous mixing. At each 30 min interval, 3 mL of aliquot was sampled, diluted with 3 mL of distilled water, and centrifuged twice at 5000 rpm for 5 min each time to remove catalyst nanoparticles. The supernatant was carefully analyzed by recording the maximum absorption band (554 nm) by a UV–vis spectrophotometer (Purkinje General T6).

Active species trapping experiments were accomplished using a similar procedure as described above, except the addition of 5.0 mM of disodium ethylenediaminetetraacetate dihydrate (EDTA-2Na), benzoquinone (BQ), or isopropanol (IPA) to detect holes (h^+), $\bullet O_2^-$, and •OH radicals, respectively [25].

3. Results and discussion

3.1. XRD patterns

X-ray diffraction patterns of CNs–TiO_2 hybrids, bare TiO_2, and CNs were exhibited in Fig. 1. The intensive diffraction peak at 27.7° of bare CNs is indexed to (0 0 2) diffraction plane for graphitic materials, relating to the characteristic interlayer stacking structure (JCPDS87-1526) [25]. Another distinct diffraction is found at nearly 13.1° and assigned as (1 0 0) diffraction plane, revealing the interplanar structural packing [26]. All diffraction peaks of bare TiO_2 are attributed to anatase phase, instead of rutile phase, which is in good accordance with the reference [27]. Diffraction patterns of CNs–TiO_2 hybrids resemble that of bare anatase TiO_2 and no characteristic peaks of CNs are observable, attributing to the low content and relatively low diffraction intensity of CNs [20]. Moreover, the absence of other diffraction peaks adequately demonstrates the high purity of synthesized hybrids without any byproducts formed.

3.2. Nitrogen adsorption

Nitrogen adsorption–desorption isotherms of CNs–TiO_2 hybrids, bare TiO_2, and CNs were depicted in Fig. 2. Present

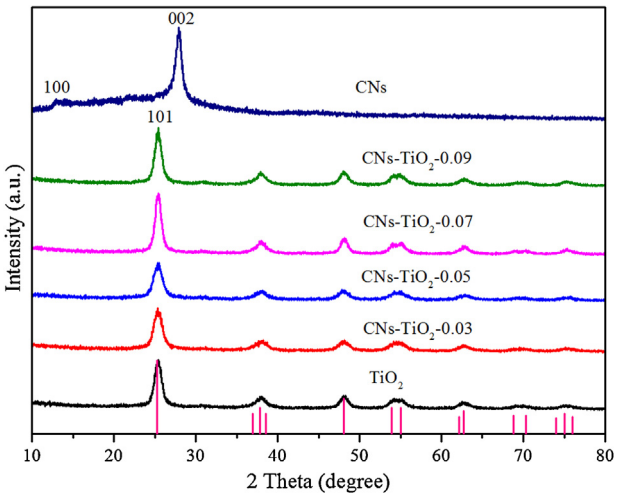

Fig. 1. XRD patterns of CNs–TiO_2 hybrids, bare TiO_2, and CNs.

isotherm of bare TiO_2 is assigned to type IV according to the IUPAC classification, displaying a H_2 hysteresis loop of a capillary condensation [19]. The feature of type IV isotherm is closely relevant to the presence of mesopores during aggregation of anatase nanoparticles [21,28], which is also identified by the average pore size of 3.43 nm calculated with the BJH method from adsorption data. The isotherm of bare CNs is classified as type IV with a H_3 hysteresis loop at a high relative pressure range of 0.7–1.0, confirming the existence of slit-like pores [21]. With the increase of CNs amount, isotherms of CNs–TiO_2 hybrids gradually vary to a shape featured with both bare TiO_2 and CNs characteristics, and specific surface areas increase to 140.1 m^2/g of CNs–TiO_2-0.05 and then decrease to 90.5 m^2/g of CNs–TiO_2-0.09, as seen in Fig. 2 and Table 1. The results indicate that the presence of appreciate amount of CNs during synthesis might influence the formation and growth of TiO_2 nanograins and further aggregation of TiO_2 nanoparticles. In addition, an appreciate amount of CNs might favor a good dispersion of CNs in hybrids, thus exerting a positive effect on the increase of specific surface areas. However, excess amount of CNs tended to self-aggregation and hereby the CNs content in hybrids decreased, causing the shrinkage of specific surface areas. It is well known that samples with enlarged surface areas readily

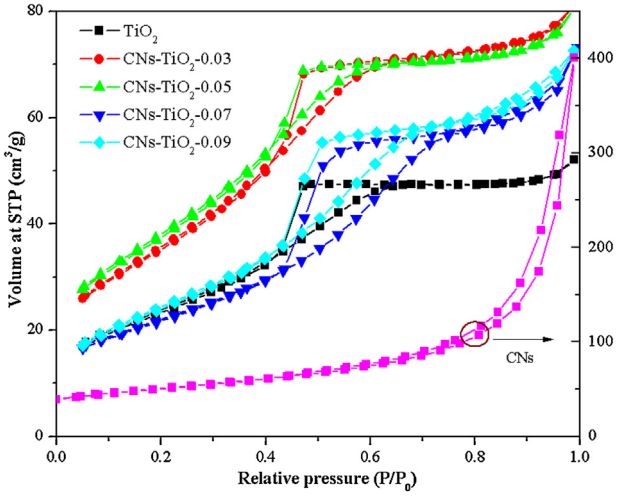

Fig. 2. N_2 adsorption–desorption isotherms of CNs–TiO_2 hybrids, bare TiO_2, and CNs.

Table 1
S_{BET}, D_{BJH}, and apparent reaction rate constant of CNs–TiO_2 hybrids, bare TiO_2, CNs, and N-TiO_2.

Samples	S_{BET} (m^2/g)	D_{BJH} (average pore diameter, nm)	Rate constant ($\times 10^{-2}$)
TiO_2	87.49	3.43	0.49
CNs–TiO_2-0.03	132.13	3.48	0.98
CNs–TiO_2-0.05	140.13	3.38	1.20
CNs–TiO_2-0.07	78.96	5.12	1.14
CNs–TiO_2-0.09	90.51	4.42	0.73
CNs	165.66	16.4	2.41
N-TiO_2	–	–	0.17

exhibit enhanced photocatalytic capability, mainly owning to the abundant active sites exposed and large light harvesting.

3.3. FT-IR spectra

FT-IR spectra were recorded to show chemical structures of CNs–TiO_2 hybrids, bare TiO_2, and CNs, as represented in Fig. 3. For the spectrum of bare CNs, two broad and pronounced peaks at 3200 cm^{-1} and 3400 cm^{-1} originate from stretching vibrations of N—H and O—H, corresponding to residual amino groups attached to sp^2 hybridized carbons and absorbed H_2O molecules on the surface, respectively [3]. Several intense adsorption peaks in the region of 1200–1640 cm^{-1} are corresponding to the typical stretching modes of aromatic CN heterocycles [29]. In addition, an apparent peak around 809 cm^{-1} is assigned to the characteristic breathing mode of triazine unites [11]. As to the spectrum of bare TiO_2, a broad band ranging from 400 cm^{-1} to 800 cm^{-1} is attributed to Ti—O—Ti stretching vibration modes [30]. All characteristic adsorption peaks of both components CNs and TiO_2 are coexisted in as-synthesized samples except the relatively low intensity of adsorption peaks of CNs in hybrids comparing to that in pristine CNs, owning to the low content of CNs in structure, as also evidenced in XRD section. Especially, the intensity of adsorption peaks at 1200–1640 cm^{-1} increased from sample CNs–TiO_2-0.03 to CNs–TiO_2-0.05 and then decreased, which is in agreement with the variation of specific surface areas as aforementioned.

3.4. XPS analysis

X-ray photoelectron spectroscopy was utilized to investigate the oxidation state and surface chemical compositions of CNs–TiO_2-0.05 hybrid, bare TiO_2, and CNs, as shown in Fig. 4. The C 1s signal was set to 284.8 eV for calibration. From the survey XPS

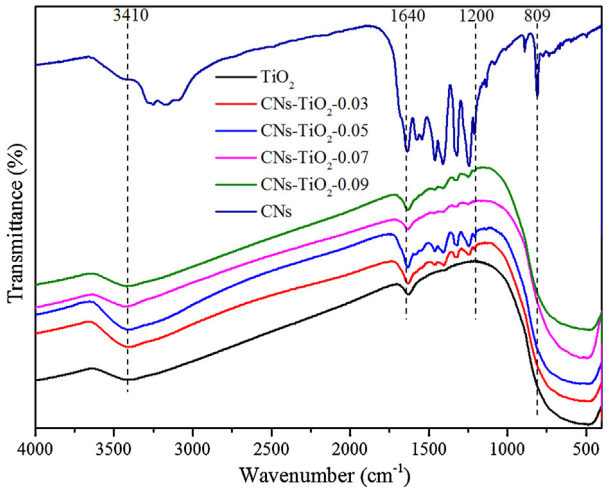

Fig. 3. FT-IR spectra of CNs–TiO_2 hybrids, bare TiO_2, and CNs.

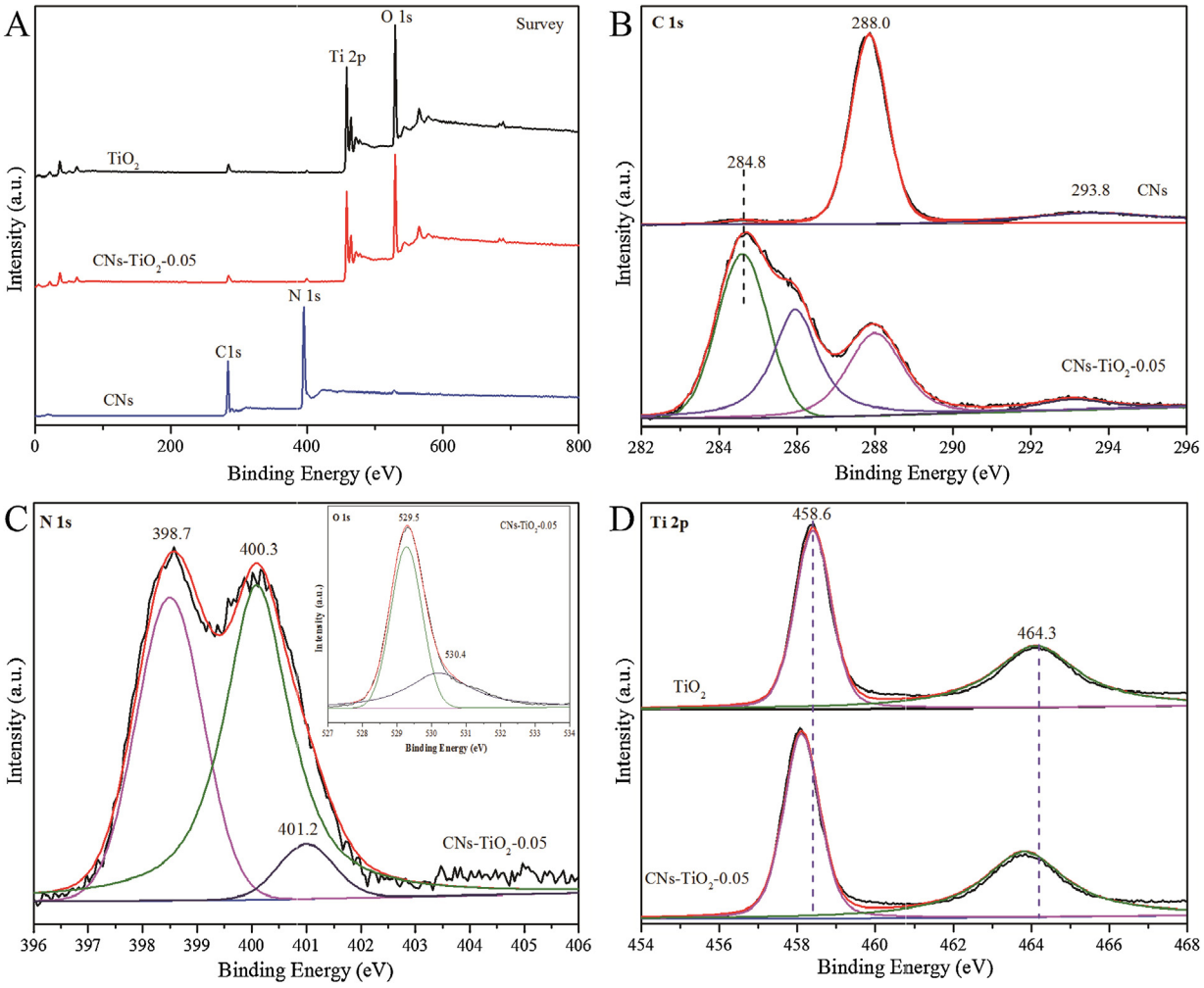

Fig. 4. X-ray photoelectron spectra of (A) survey scan of CNs–TiO_2-0.05 hybrid, bare TiO_2, and CNs; high-resolution spectra of (B) C 1s of CNs–TiO_2-0.05 hybrid and bare CNs, (C) N 1s and O 1s (inset) of CNs–TiO_2-0.05 hybrid, and (D) Ti 2p of CNs–TiO_2-0.05 hybrid and bare TiO_2.

spectrum in Fig. 4A, it is obvious that C and N elements are observable in CNs–TiO_2-0.05 hybrid, though the intensity of them is quite low in comparison with that of bare CNs. The results confirm the presence of low content of CNs in CNs–TiO_2-0.05 hybrid, which is in good accordance with the FT-IR and XRD analysis. In addition, atomic percent of elements C, N, Ti, and O for all CNs–TiO_2 hybrids were also tested and collected in Table S1 (Supporting section). It is evident that all samples contain both phase of CNs and TiO_2 and atomic percent of C and N is improved with the increase of CNs amount up to 5% and then reduced, in good agreement with the variation of adsorption peak intensities in FT-IR spectra and specific surface areas. High-resolution spectra of C 1s, N 1s, Ti 2p, and O 1s were displayed in following Fig. 4B–D.

As to bare CNs in Fig. 4B, the C 1s XPS spectrum shows three main peaks at around 284.8 eV, 288.0 eV, and 293.8 eV, corresponding to the adventitious carbon, C—$(N)_3$ group of CNs, and carbon in aromatic rings connected with terminal uncondensed amino groups [22]. The last two peaks are typical features of basic tri-*s*-triazine units in CNs [31]. For CNs–TiO_2-0.05 hybrid, beside three peaks described above, another pronounced peak is also detected at 286.2 eV, attributing to the sp^2 carbon atoms bonded to N inside aromatic units [32]. It is clear that intensity ratio of peaks positioned at 288.0 eV to 284.8 eV in CNs–TiO_2-0.05 hybrid is remarkably low comparing with that of bare CNs, again proving the presence of CNs in hybrids with low content [21].

The high-resolution XPS spectra of N 1s and O 1s of CNs–TiO_2-0.05 hybrid were displayed in Fig. 4C. Several signals of N 1s located at 398.7 eV, 400.3 eV, and 401.2 eV are present and originate from sp^2 bonded N in triazine rings, tertiary N in N—$(C)_3$ groups, and N atoms in amino moieties, owning to the existence of CNs in hybrid [28]. In addition, O 1s peaks (inset of Fig. 4C) centered at 529.5 eV and 530.4 eV are attributed to O atoms in Ti—O and surface OH [22,28], respectively.

Ti 2p Spectrum in bare TiO_2 are composed of two peaks corresponding to Ti $2p_{3/2}$ and Ti $2p_{1/2}$ with binding energy of 458.6 eV and 464.3 eV, ascribing to Ti^{4+} species in TiO_2 aggregations. However, a small shift around 0.3 eV toward low binding energy region was found for both Ti $2p_{3/2}$ and Ti $2p_{1/2}$ after hybridization of TiO_2 with CNs, which is possibly due to the partial substitution of Ti—O with Ti—N and resultant enhanced electron density on Ti as a consequence of relatively small electronegativity of N comparing with O [33], indicating that chemical binding between two components was possibly formed instead of a simply physical mixture.

3.5. *UV–vis DRS*

The optical property of CNs–TiO_2-0.05 hybrid, bare TiO_2, and CNs was measured by UV–vis diffuse reflectance spectroscopy and showed in Fig. 5A. The UV–vis DRS spectrum of CNs–TiO_2-0.05 hybrid is quite similar to that of bare TiO_2 but the main

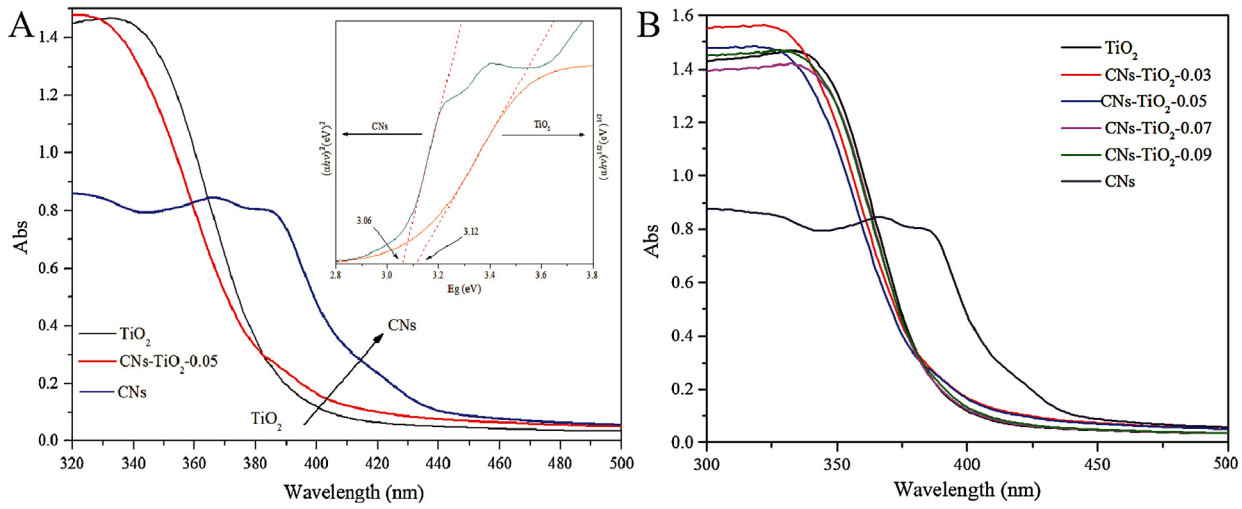

Fig. 5. (A) UV–vis absorption spectra of CNs–TiO_2-0.05 hybrid, bare TiO_2, and CNs ($(\alpha h\nu)^2$ or $(\alpha h\nu)^{1/2}$ versus E_g plot of bare CNs and TiO_2, inset); (B) UV–vis absorption spectra of CNs–TiO_2 hybrids, bare TiO_2, and CNs.

adsorption edge of CNs–TiO_2-0.05 hybrid moves toward the visible light region, as evidenced in Fig. 5A. In addition, the adsorption of CNs–TiO_2-0.05 hybrid is slightly strengthened beyond 400 nm. Band gap energies of CNs and TiO_2 could be estimated as 3.06 eV and 3.12 eV from a plot of $(\alpha h\nu)^2$ or $(\alpha h\nu)^{1/2}$ versus E_g, respectively, as depicted in the inset of Fig. 5A. For comparison, UV–vis DRS spectra of all CNs–TiO_2 hybrids were evaluated and displayed in Fig. 5B. Hybrid CNs–TiO_2-0.03 and CNs–TiO_2-0.05 exhibit relatively strengthened adsorption over 400 nm, comparing to other samples, maybe relating to the higher content and better dispersion of CNs in structures. Visible light responsive catalysts with strong adsorption capability ensure the efficient utilization of visible light and enhanced photoinduced electron–holes separation, consequently causing improved photocatalytic performance [34].

3.6. Microstructure analysis

The morphology and microstructure of CNs–TiO_2-0.05 hybrid, bare TiO_2, and CNs were recorded by TEM and SEM, as shown

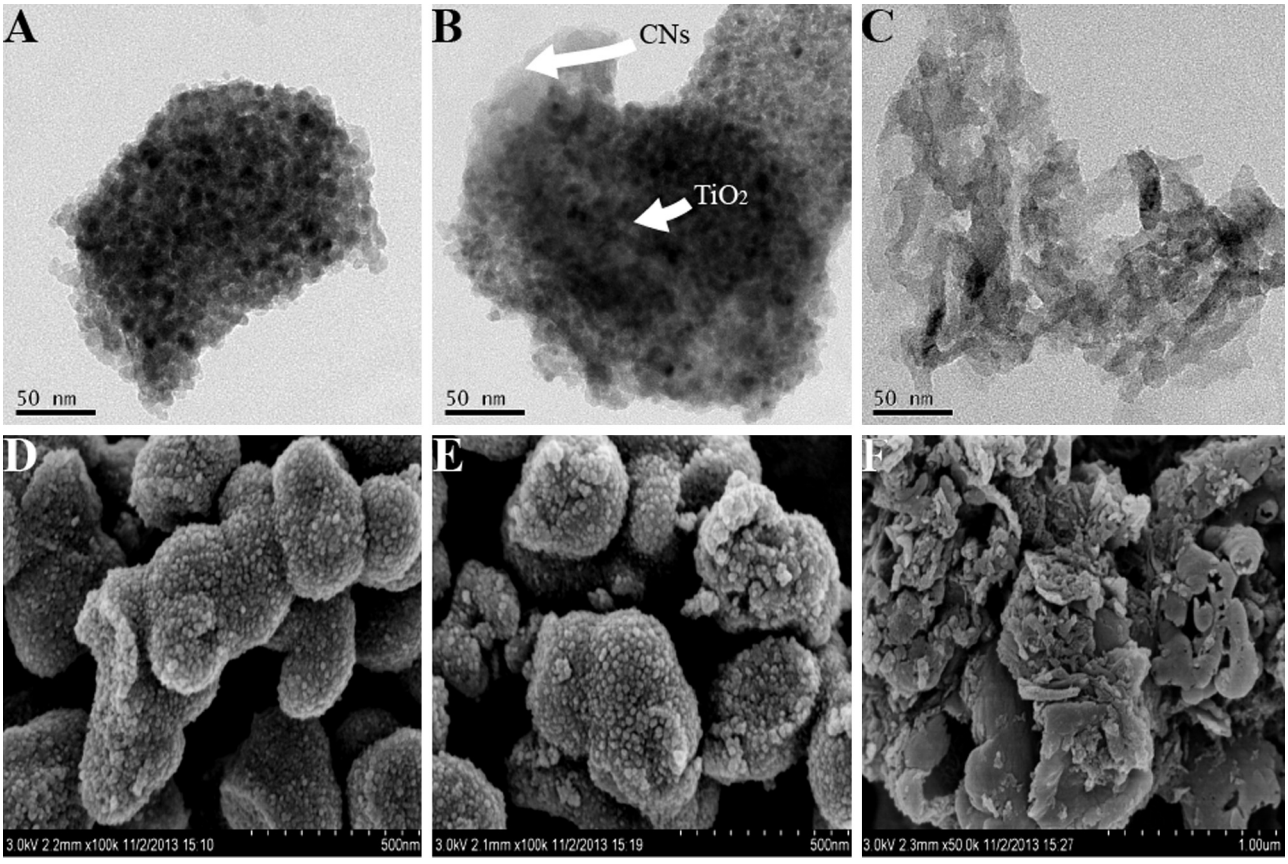

Fig. 6. TEM images of (A) bare TiO_2, (B) CNs–TiO_2-0.05 hybrid, and (C) CNs; SEM images of (D) bare TiO_2, (E) CNs–TiO_2-0.05 hybrid, and (F) CNs.

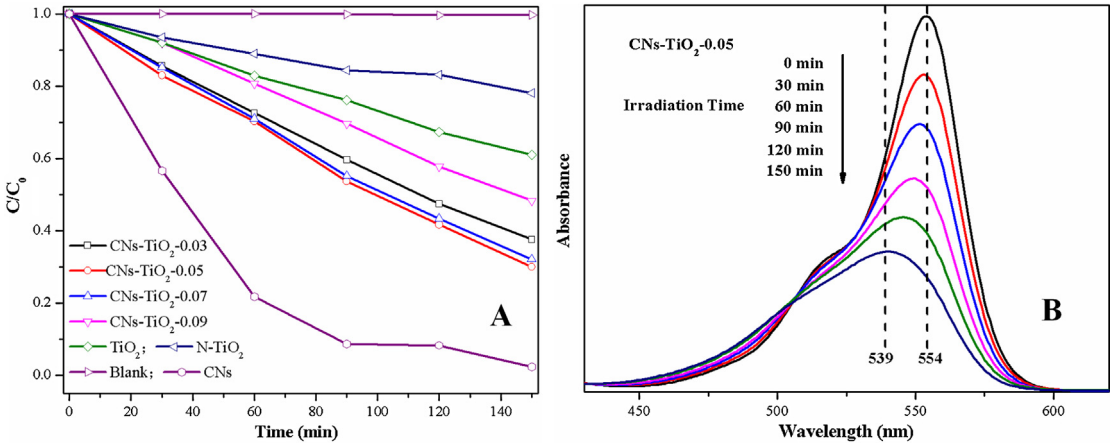

Fig. 7. (A) Photocatalytic activity for the degradation of RhB under visible light irradiation on CNs–TiO_2 hybrids, bare TiO_2, CNs, and N-TiO_2; (B) the variation of the RhB main adsorption peak with extension of irradiation time.

in Fig. 6. It is observable that bare TiO_2 aggregated into small regular roundish particles of about 15–20 nm with a homogeneous size distribution in Fig. 6A. These roundish particles further assembled to microsized clusters with coarse surface and loose structure in Fig. 6D, during which mesopores were generated. The bare CNs exfoliated exhibit lamellar structures with smooth surface and crimpled edges, as evidenced in Fig. 6C and F. The SEM image of CNs–TiO_2-0.05 hybrid in Fig. 6E resembles that of bare TiO_2, indicating the main structure of bare TiO_2 could be retained after hybridization. In addition, both roundish particles of TiO_2 and lamellar CNs with smooth surface at the boundary can be observed in Fig. 6B and each signed with an arrow. The microstructure analysis indicates that both components are closely attached to form the heterojunction interface along boundaries, by which photoinduced charge carriers can be easily migrated and separated [35].

3.7. Photocatalytic measurements

Photocatalytic performances of CNs–TiO_2 hybrids with variable CNs amount were accessed by degradation of dye RhB under visible light irradiation and shown in Fig. 7A. Direct photolysis of RhB is almost negligible and bare TiO_2 show a relatively low catalytic efficiency mainly through a photosensitive pathway [36]. CNs displayed a best catalytic performance among all samples tested. With a dramatically enlarged specific surface area after exfoliation, CNs has been proven as an efficient photocatalyst that is much better than bulk g-C_3N_4 upon identical conditions [17]. Therefore, CNs is a good alternative to construct TiO_2 hybrids with merits of visible light response and enhanced catalytic performance. The as-synthesized CNs–TiO_2 hybrids exhibit much higher photocatalytic outcomes than bare TiO_2 and N–TiO_2. The photocatalytic efficiencies of CNs–TiO_2 hybrids enhance in line with the increase of CNs amount from 3% to 5% in hybrids and inversely decayed if CNs amount is further increased beyond 5%. CNs–TiO_2-0.05 hybrid is the best candidate among all CNs–TiO_2 hybrids upon photocatalytic degradation of RhB. The experimental data were fitted with a pseudo-first-order model to study reaction kinetics of RhB degradation and CNs–TiO_2-0.05 hybrid showed the largest reaction rate among all CNs–TiO_2 hybrids that is nearly 2.4 times and 7.0 times that of bare TiO_2 and N-TiO_2, as seen in Table 1. In addition, blue shift of the main adsorption of RhB 554 nm to 539 nm in Fig. 7B was found along with the extension of irradiation time and could be attributed to a stepwise deethylation of RhB [36].

The enhanced photocatalytic ability is relevant to the formation of heterojunction structures between both components, which can efficiently promote the transfer and separation of charge carries via smooth interface, thus enhancing the photocatalytic efficiency. To construct an effective hybrid, appropriate amount of CNs was extraordinarily required, which would be explained as follows. First, proper amount of CNs added might enhance the specific surface area and extend the light adsorption [13], as evidenced in Table 1. Materials with enlarged surface areas are prone to absorb more organic pollutants on the surface that tend to subsequently degrade by a larger number of active sites. Another factor is possibly associated with the optical property of CNs–TiO_2 hybrids. As aforementioned, the main adsorption edge and adsorption in UV–vis DRS spectra are variable with the increase of CNs content. Both merits of suitable specific surface area and favorable optical property in CNs–TiO_2-0.05 hybrid may be crucial to achieve the best catalytic outcome upon identical conditions. Second, TiO_2 can assemble to a unique structure with mesopores of uniformed size distribution even hybridizing with CNs [22]. The mesopored structure facilitated multiple-reflection of visible light, thus enhancing the light harvesting. Besides, mesopores structure was beneficial to the mass transfer of pollutants and degraded products. As a result, the enhanced catalytic efficiency could be mainly attributed to the well-matched band gap structure with heterojunction interface, suitable specific surface area, and favorable optical property.

3.8. Photocatalytic mechanism

In order to understand the photocatalytic mechanism, active species trapping experiments were conducted through introducing

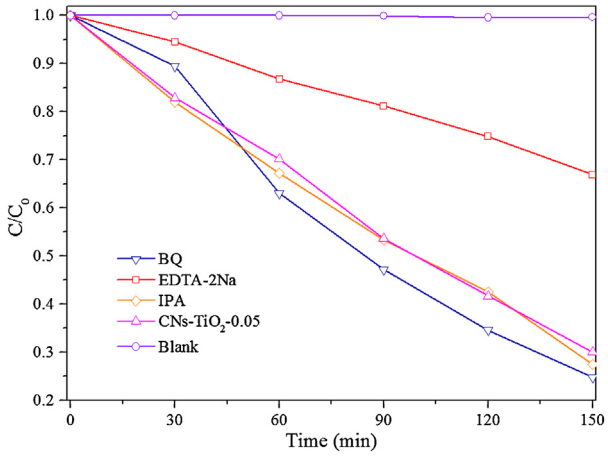

Fig. 8. Active species trapping experiments of CNs–TiO_2-0.05 hybrid.

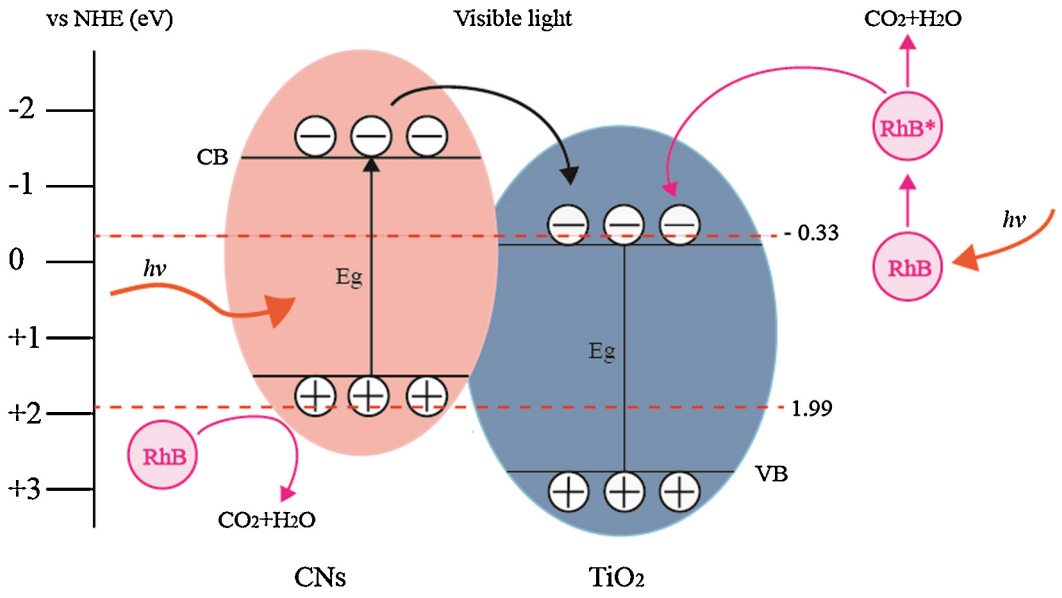

Fig. 9. Proposed mechanism of CNs–TiO_2 hybrids upon visible light irradiation.

reagents BQ, EDTA-2Na, and IPA to quench $\bullet O_2^-$, h^+, and •OH species, respectively [37]. It is found that the addition of BQ and IPA have almost no effect on the degradation results, revealing that both active species $\bullet O_2^-$ and •OH may impossibly be generated during reaction. The holes h^+ played an important role on the photocatalysis as a result of greatly depressed catalytic efficiency after addition of holes quencher EDTA-2Na, as shown in Fig. 8.

According to the simple approach [22], the CB and VB potentials of CNs were estimated at −1.30 eV and 1.76 eV, and the CB and VB potentials of TiO_2 were −0.25 eV and 2.87 eV. Under irradiation, CNs could absorb visible light and be easily excited to provide holes and electrons. The photogenerated holes and electrons were located at VB and CB, respectively. However, TiO_2 failed to be excited because of the large band gap energy therefore the hole–electron pairs were impossible to form [36]. Since the potential of CB of CNs (−1.30 eV) was more negative than that of TiO_2 (−0.25 eV), electrons on CB of CNs were of easy to transfer across the smooth heeterojunction interface and reach the CB of TiO_2. In addition, RhB, as a photosensitive reagent, inclined to harvest visible light to produce electrons, which could also be injected to CB of TiO_2 since the lowest molecular orbital potential of RhB (−0.75 eV) was more negative than CB potential (−0.25 eV) of TiO_2. The RhB molecules on excited state after donating electrons tended to self-degrade or degrade other RhB molecules on ground state [36,38]. The electrons on CB of TiO_2 were insufficient to react with adsorbed molecular oxygen to generate $\bullet O_2^-$ species since the potential of CB of TiO_2 is less negative than $O_2/\bullet O_2^-$ couple (−0.33 eV) [22], which was in good accordance with the trapping experiments. In addition, the holes stayed on VB of CNs because the potential of VB of CNs was more negative than that of TiO_2. Consequently, electrons and holes were separated and located on CB of TiO_2 and VB of CNs, greatly prolonging the life of electrons and thus inhibiting recombination rate, finally remarkably enhancing the photocatalytic efficiency. Holes on VB of CNs were unable to oxidize OH^- or H_2O molecules to form •OH species owning to the less negative of VB (1.76 eV) on CNs than that of $OH^-/\bullet OH$ couple (1.99 eV) [22]. Thereby, holes had a tendency to oxidize pollutants directly without producing other active species, which was proven by trapping experiments as well. Based upon the discussion, it is reasonable that the mechanism in this study may combine two pathways, called as photosensitive route and photocatalytic route, as described in detail in Fig. 9.

4. Conclusions

In summary, a series of CNs–TiO_2 hybrids were synthesized through a facile sol–gel method. Structural analyses indicated that both components were present and close in contact to form heterojunction structures. The as-synthesized CNs–TiO_2 hybrids exhibited much higher photocatalytic efficiency in terms of depredating dye RhB, mainly attributing to the well-matched band gap structure with heterojunction interface, suitable specific surface area, and favorable optical property. Especially, the best candidate CNs–TiO_2-0.05 hybrid showed an apparent reaction rate constant 2.4 times and 7 times that of bare TiO_2 and N-TiO_2 under identical conditions. Finally, a possible photocatalytic mechanism was also proposed on the basis of active species trapping experiments.

Acknowledgments

We are grateful to the National Natural Science Foundation of China (grant number 21207089 and 41076040), the project-sponsored by SRF for ROCS, SEM., and the 863 project (grant number 2013AA06A207-1) for financial support.

Appendix A. Supplementary data

Supplementary data associated with this article can be found, in the online version, at http://dx.doi.org/10.1016/j.apsusc.2014.05.111.

References

[1] M.R. Hoffmann, S.T. Martin, W. Choi, D.W. Bahnemann, Environmental applications of semiconductor photocatalysis, Chem. Rev. 95 (1995) 69–96.
[2] T.L. Thompson, J.T. Yates, Surface science studies of the photoactivation of TiO_2 new photochemical processes, Chem. Rev. 106 (2006) 4428–4453.
[3] H. Yan, H. Yang, TiO_2–g-C_3N_4 composite materials for photocatalytic H_2 evolution under visible light irradiation, J. Alloys Compd. 509 (2011) L26–L29.
[4] J. Xu, Y. Ao, D. Fu, C. Yuan, Synthesis of Gd-doped TiO_2 nanoparticles under mild condition and their photocatalytic activity, Colloids Sur., A: Physicochem. Eng. Aspects 334 (2009) 107–111.
[5] F. Lin, D. Jiang, X. Ma, The effect of milling atmospheres on photocatalytic property of Fe-doped TiO_2 synthesized by mechanical alloying, J. Alloys Compd. 470 (2009) 375–378.
[6] P. Reddy, P. Reddy, V. Sharma, B. Srinivas, V. Kumari, M. Subrahmanyam, Photocatalytic degradation of isoproturon pesticide on C, N and S doped TiO_2, J. Water Resour. Prot. 2 (2010) 235–244.

[7] G. Yang, Z. Yan, T. Xiao, Low-temperature solvothermal synthesis of visible-light-responsive S-doped TiO_2 nanocrystal, Appl. Surf. Sci. 258 (2012) 4016–4022.
[8] A. Dodd, A. McKinley, T. Tsuzuki, M. Saunders, Optical and photocatalytic properties of nanoparticulate $(TiO_2)_x(ZnO)_{1-x}$ powders, J. Alloys Compd. 489 (2010) L17–L21.
[9] Y. Liu, F. Xin, F. Wang, S. Luo, X. Yin, Synthesis, characterization, and activities of visible light-driven Bi_2O_3–TiO_2 composite photocatalysts, J. Alloys Compd. 498 (2010) 179–184.
[10] X. Wang, K. Maeda, A. Thomas, K. Takanabe, G. Xin, J. Carlsson, K. Domen, M. Antonietti, A metal-free polymeric photocatalyst for hydrogen production from water under visible light, Nat. Mater. 8 (2009) 76–80.
[11] A. Thomas, A. Fischer, F. Goettmann, M. Antonietti, J. Müller, R. Schlögl, J. Carlsson, Graphitic carbon nitride materials: variation of structure and morphology and their use as metal-free catalysts, J. Mater. Chem. 18 (2008) 4893–4908.
[12] Y. Wang, X. Wang, M. Antonietti, Polymeric graphitic carbon nitride as a heterogeneous organocatalyst: from photochemistry to multipurpose catalysis to sustainable chemistry, Angew. Chem. Int. Ed. 51 (2012) 68–89.
[13] J. Xu, L. Zhang, R. Shi, Y. Zhu, Chemical exfoliation of graphitic carbon nitride for efficient heterogeneous photocatalysis, J. Mater. Chem. A 1 (2013) 14766–14772.
[14] Y. Wang, J. Hong, W. Zhang, R. Xu, Carbon nitride nanosheets for photocatalytic hydrogen evolution: remarkably enhanced activity by dye sensitization, Catal. Sci. Technol. 3 (2013) 1703–1711.
[15] J. Tian, Q. Liu, C. Ge, Z. Xing, A. Asiri, A. Al-Youbi, X. Sun., Ultrathin graphitic carbon nitride nanosheets: a low-cost, green, and highly efficient electrocatalyst toward the reduction of hydrogen peroxide and its glucose biosensing application, Nanoscale 5 (2013) 8921–8924.
[16] P. Niu, L. Zhang, G. Liu, H. Cheng, Graphene-like carbon nitride nanosheets for improved photocatalytic activities, Adv. Funct. Mater. 22 (2012) 4763–4770.
[17] M. Zhang, J. Xu, R. Zong, Y. Zhu, Enhancement of visible light photocatalytic activities via porous structure of g-C_3N_4, Appl. Catal., B: Environ. 147 (2014) 229–235.
[18] N. Yang, G. Li, W. Wang, X. Yang, W. Zhang, Photophysical and enhanced daylight photocatalytic properties of N-doped TiO_2/g-C_3N_4 composites, J. Phys. Chem. Solids 72 (2011) 1319–1324.
[19] C. Miranda, H. Mansilla, J. Yáñez, S. Obregón, G. Colón, Improved photocatalytic activity of g-C_3N_4/TiO_2 composites prepared by a simple impregnation method, J. Photochem. Photobiol., A: Chem. 253 (2013) 16–21.
[20] S. Zhao, S. Chen, H. Yu, X. Quan, g-C_3N_4/TiO_2 hybrid photocatalyst with wide absorption wavelength range and effective photogenerated charge separation, Sep. Purif. Technol. 99 (2012) 50–54.
[21] J. Yu, S. Wang, J. Low, W. Xiao, Enhanced photocatalytic performance of direct Z-scheme g-C_3N_4–TiO_2 photocatalysts for the decomposition of formaldehyde in air, Phys. Chem. chem. Phys. 15 (2013) 16883–16890.
[22] N. Boonprakob, N. Wetchakun, S. Phanichphant, D. Waxler, P. Sherrell, A. Nattestad, J. Chen, B. Inceesungvorn, Enhanced visible-light photocatalytic activity of g-C_3N_4/TiO_2 films, J. Colloid Int. Sci. 417 (2014) 402–409.
[23] T. Li, L. Zhao, Y. He, J. Cai, M. Luo, J. Lin, Synthesis of g-C_3N_4/$SmVO_4$ composite photocatalyst with improved visible light photocatalytic activities in RhB degradation, Appl. Catal., B: Environ. 129 (2013) 255–263.
[24] Q. Truong, T. Le, J. Liu, C. Chung, Y. Ling, Synthesis of TiO_2 nanoparticles using novel titanium oxalate complex towards visible light-driven photocatalytic reduction of CO_2 to CH_3OH, Appl. Catal., A: Gen. 437–438 (2012) 28–35.
[25] L. Ye, J. Liu, Z. Jiang, T. Peng, L. Zan, Facets coupling of BiOBr–g-C_3N_4 composite photocatalyst for enhanced visible-light-driven photocatalytic activity, Appl. Catal., B: Environ. 142–143 (2013) 1–7.
[26] F. Goettmann, A. Fischer, M. Antonietti, A. Thomas, Chemical synthesis of mesoporous carbon nitrides using hard templates and their use as a metal-free catalyst for Friedel–Crafts reaction of benzene, Angew. Chem. Int. Ed. 45 (2006) 4467–4471.
[27] Y. Ao, J. Xu, D. Fu, X. Shen, C. Yuan, Low temperature preparation of anatase TiO_2-coated activated carbon, Colloids Surf., A: Physicochem. Eng. Aspects 312 (2008) 125–130.
[28] M. Fu, J. Pi, F. Dong, Q. Duan, H. Guo, A cost-effective solid-state approach to synthesize g-C_3N_4 coated TiO_2 nanocomposites with enhanced visible light photocatalytic activity, Int. J. Photoenergy 2013 (2013) 1–7.
[29] V. Khabashesku, J. Zimmerman, J. Margrave, Powder synthesis and characterization of amorphous carbon nitride, Chem. Mater. 12 (2000) 3264–3270.
[30] J. Yu, H. Yu, B. Cheng, X. Zhao, J. Yu, W. Ho, The effect of calcination temperature on the surface microstructure and photocatalytic activity of TiO_2 thin films prepared by liquid phase deposition, J. Phys. Chem. B 107 (2003) 13871–13879.
[31] A. Vinu, Two-dimensional hexagonally-ordered mesoporous carbon nitrides with tunable pore diameter, surface area and nitrogen content, Adv. Funct. Mater. 18 (2008) 816–827.
[32] X. Zhou, B. Jin, L. Li, F. Peng, H. Wang, H. Yu, Y. Fang, A carbon nitride/TiO_2 nanotube array heterojunction visible-light photocatalyst: synthesis, characterization, and photoelectrochemical properties, J. Mater. Chem. 22 (2012) 17900–17905.
[33] X. Wang, W. Yang, F. Li, Y. Xue, R. Liu, Y. Hao, In situ microwave-assisted synthesis of porous N–TiO_2/g-C_3N_4 heterojunctions with enhanced visible-light photocatalytic properties, Ind. Eng. Chem. Res. 52 (2013) 17140–17150.
[34] L. Zhang, D. Jing, X. She, H. Liu, D. Yang, Y. Lu, J. Li, Z. Zheng, L. Guo, Heterojunctions in g-C_3N_4/TiO_2(B) nanofibres with exposed (0 0 1) plane and enhanced visible-light photoactivity, J. Mater. Chem. A 2 (2014) 2071–2078.
[35] L. Gu, J. Wang, Z. Zou, X. Han, Graphitic- C_3N_4-hybridized TiO_2 nanosheets with reactive {0 0 1} facets to enhance the UV- and visible-light photocatalytic activity, J. Hazard. Mater. 268 (2014) 216–223.
[36] T. Wu, G. Liu, J. Zhao, H. Hidaka, N. Serpone, Photoassisted degradation of dye pollutants. V. Self-photosensitized oxidative transformation of rhodamine B under visible light irradiation in aqueous TiO_2 dispersions, J. Phys. Chem. B 102 (1998) 5845–5851.
[37] T. Li, G. Chen, C. Zhou, Z. Shen, R. Jin, J. Sun, New photocatalyst BiOCl/BiOI composites with highly enhanced visible light photocatalytic performances, Dalton Trans. 40 (2011) 6751–6758.
[38] C. Chen, W. Ma, J. Zhao, Semiconductor-mediated photodegradation of pollutants under visible-light irradiation, Chem. Soc. Rev. 39 (2010) 4206–4219.